[40] C. Galletti and P. Fanghella, "Single-loop kinematotropic mechanisms," *Mech. Mach. Theory*, vol. 36, no. 3, pp. 437–450, 2009.
[41] P. Fanghella, C. Galletti, and E. Giannotti, "Parallel robots that change their group of motion," in *Advances in Robot Kinematics*. The Netherlands: Springer, 2006, pp. 49–56.
[42] S. Refaat, J. M. Hervé, S. Nahavandi, and H. Trinh, "Two-mode over-constrained three-dofs rotational-translational linear-motor-based parallel-kinematics mechanism for machine tool applications," *Robotica*, vol. 25, no. 4, pp. 461–466, 2007.
[43] X. W. Kong, C. M. Gosselin, and P. L. Richard, "Type synthesis of parallel mechanisms with multiple operation modes," *ASME J. Mech. Des.*, vol. 129, no. 6, pp. 595–601, 2007.
[44] D. Zlatanov, I. A. Bonev, and C. M Gosselin, "Constraint singularities of parallel mechanisms," in *Proc. IEEE Int. Conf. Robot. Autom.*, Washington, D.C., 2002, pp. 496–502.
[45] D. Zlatanov, I. A. Bonev, and C. M Gosselin, "Constraint singularities as c-space singularities," in *Advances in Robot Kinematics*, J. Lenarcic and F. Thomas, Eds. Dordrecht, The Netherlands: Kluwer, 2002, pp. 183–192.
[46] K. H. Hunt, "Constant-velocity shaft couplings: A general theory," *J. Eng. Ind.*, vol. 95B, no. 2, pp. 455–464, 1973.

Swedish Wheeled Omnidirectional Mobile Robots: Kinematics Analysis and Control

Giovanni Indiveri

***Abstract*—Swedish wheeled robots have received growing attention over the last few years. Their kinematic models have interesting properties in terms of mobility and possible singularities. This paper addresses the issue of kinematic modeling, singularity analysis, and motion control for a generic vehicle equipped with N Swedish wheels.**

***Index Terms*—Mobile robot kinematics, mobile robots, motion control, wheeled robots.**

I. Introduction

In the last few years, Swedish wheeled omnidirectional mobile robots have received growing attention among the mobile robotics research community. A Swedish wheel differs from a common wheel in the fact that rollers are mounted on its perimeter (see Fig. 1). If all the rollers are parallel to each other and misaligned with respect to the wheel hub axis, they will provide an extra degree of mobility with respect to a traditional perfectly rolling wheel.

The wheels depicted in Fig. 1 are often called mecanum or Swedish wheels: one of their design parameters is the angle γ between the rollers rolling direction $\mathbf{g}$ and the wheel hub axis direction $\mathbf{h}$. Typical values are $\gamma = 45^\circ$ and $\gamma = 0^\circ$, as shown in Fig. 1 (left and right cases, respectively). Note that the degenerate case $\gamma = 90^\circ$ has no practical interest as it would allow the same mobility of traditional wheels. In the literature, wheels with $\gamma = 45^\circ$ are more often called mecanum wheels whereas the ones with $\gamma = 0^\circ$ are generally called Swedish wheels. In the following, the term Swedish wheel will denote the general case for some fixed γ. As reported in [1], the mecanum wheel was invented in 1973 by Bengt Ilon, an engineer working for the Swedish company Mecanum AB. Since then, this wheel design has attracted the attention of the mobile robotics research community. The interest in such kind of wheels is related to the possibility of developing omnidirectional robots in the sense of [2], i.e., robots that "have a full mobility in the plane meaning thereby that they can move at each instant in any direction without any reorientation" [2]. The need to reorient the wheels or not prior to implementing any desired linear velocity is related to the presence or not of nonholonomic constraints [3], [4]. Since the early study of Agulló *et al.* [5], the kinematics analysis of Swedish or mecanum wheel robots has been addressed in several papers [6]–[12]. All these except the study of Agulló *et al.* [5] and Saha et al. [9] consider either three or four Swedish wheeled robots for some value of γ. One of the objectives of this paper is to derive, in the most general setting of N Swedish wheels with fixed (but arbitrary) roller wheel angle, necessary and sufficient geometrical conditions on relative wheel arrangement that guarantee: 1) the absence of singularities and 2) the possibility of decoupling commanded linear and angular robot velocities. This kind of information can be most valuable to guide the design of the robot *a priori*. The results obtained addressing the N-wheel case, besides realizing at once a unified analysis of the most common three- and four-wheel designs, allow to easily explore, for example, possible six-wheel designs that have a large interest in the field of outdoor and rough terrain applications [14]. As a side result of the proposed analysis, all possible kinematics singularities occurring as a function of the roller–wheel angle and wheel arrangement—can be identified. Moreover, building on well-known methods, the trajectory tracking and pose regulation problems are solved for these systems taking explicitly into account actuator velocity saturation.

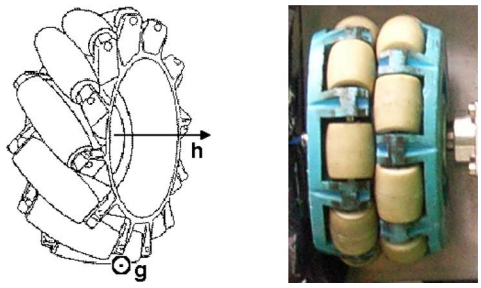

Fig. 1. Mecanum wheel: $\gamma = 45^\circ$ (left) and $\gamma = 0^\circ$ (right).

The paper is organized as follows: the general kinematics model for an N Swedish wheeled vehicle is derived in Section II. The guidance trajectory tracking and pose regulation control problems in the presence of actuator velocity saturationare addressed in Section III. Experimental results are reported in Section IV. At last, some concluding remarks are addressed in Section V.

II. Kinematics Model

With reference to Fig. 2, for the sake of introducing the notation, a three-wheel omnidrive mobile robot is considered. All wheel main axes, i.e., hub axes, are assumed to always lie parallel to the fixed ground plane $\mathcal{P}$ having unit vector $\mathbf{k} \perp \mathcal{P}$. Each of the N Swedish wheels is indexed from 1 to N: for the hth wheel, the roller in contact with the ground plane $\mathcal{P}$ is depicted as an ellipse with main axes oriented along the unit vectors $\mathbf{n}_{\gamma h} : \|\mathbf{n}_{\gamma h}\| = 1$ and $\mathbf{u}_{\gamma h} : \|\mathbf{u}_{\gamma h}\| = 1$.

Manuscript received June 27, 2008; revised October 6, 2008 and November 19, 2008. First published January 21, 2009; current version published February 4, 2009. This paper was recommended for publication by Associate Editor F. Lamiraux and Editor W. K. Chung upon evaluation of the reviewers' comments.

G. Indiveri is with the Dipartimento Ingegneria Innovazione, University of Salento, 73100 Lecce, Italy (e-mail: giovanni.indiveri@unile.it).

Color versions of one or more of the figures in this paper are available online at http://ieeexplore.ieee.org.

Digital Object Identifier 10.1109/TRO.2008.2010360

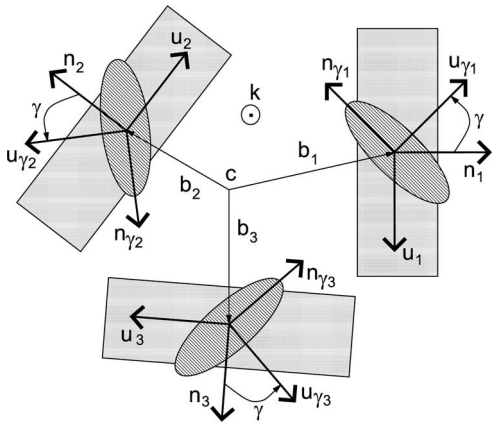

Fig. 2. Three-wheel omnidrive robot: geometrical model.

The unit vector $\mathbf{n}_{\gamma h}$ is aligned with the roller's rolling axis on the main wheel perimeter and $\mathbf{u}_{\gamma h} := \mathbf{n}_{\gamma h} \times \mathbf{k}$ indicates the instantaneous tangent velocity direction of the roller associated with its rotation around $\mathbf{n}_{\gamma h}$. All wheels are assumed to be identical and have the same radius ρ. The position of the hth wheel in the body-fixed frame is denoted by $\mathbf{b}_h$. The unit vector of each wheel hub axis, i.e., the unit vector of the wheel's main rotation axis, is denoted by $\mathbf{n}_h : \|\mathbf{n}_h\| = 1$. At last for each wheel, the unit vector $\mathbf{u}_h := \mathbf{n}_h \times \mathbf{k}$ is defined indicating the instantaneous tangent velocity direction of the wheel as a consequence of its rotation around $\mathbf{n}_h$. Note that with reference to Fig. 1, the unit vectors $\mathbf{u}_{\gamma h}$ and $\mathbf{n}_h$ would correspond to $\mathbf{g}$ and $\mathbf{h}$, respectively. In the given hypothesis, all the introduced vectors except $\mathbf{k}$ are parallel to the ground plane $\mathcal{P}$.

Given the components of any two 3-D vectors $\mathbf{a}$ and $\mathbf{b}$ on a common orthonormal frame, their vector product will be computed using the skew-symmetric matrix $S(\cdot)$ such that

$$\mathbf{a} \times \mathbf{b} = S(\mathbf{a})\,\mathbf{b}. \tag{1}$$

Calling $\mathbf{v}_c$ the linear velocity of the robots center (indicated as point c in Fig. 2) and $\omega\,\mathbf{k}$ its angular velocity vector, the velocity vector $\mathbf{v}_h$ of the center of each omnidirectional wheel hub will be given by

$$\mathbf{v}_h = \mathbf{v}_c + \omega\,\mathbf{k} \times \mathbf{b}_h, \qquad h = 1, 2, 3, \ldots, N. \tag{2}$$

Considering the generic hth wheel and dropping for the time being the index h for the sake of notational clarity, in the case of perfect rolling, the velocity $\mathbf{v} = \mathbf{v}_h$ given by (2) will be physically realized by the roller rotation around $\mathbf{n}_\gamma$ and the wheel rotation around $\mathbf{n}$. Namely, assuming that $\mathbf{n}_\gamma$ and $\mathbf{n}$ are *not* aligned, i.e., $\gamma \neq (2\nu + 1)90^\circ$, where ν is an integer

$$\mathbf{v} \;=\; \alpha\,\mathbf{u}_\gamma \;+\; \beta\,\mathbf{u}$$

implying

$$\mathbf{n}^T\mathbf{v} \;=\; \alpha\,\left(\mathbf{n}^T\mathbf{u}_\gamma\right)$$
$$\mathbf{n}_\gamma^T\mathbf{v} \;=\; \beta\,\left(\mathbf{n}_\gamma^T\mathbf{u}\right)$$

and consequently

$$\mathbf{v} \;=\; \frac{\mathbf{n}^T\mathbf{v}}{\mathbf{n}^T\mathbf{u}_\gamma}\;\mathbf{u}_\gamma \;+\; \frac{\mathbf{n}_\gamma^T\mathbf{v}}{\mathbf{n}_\gamma^T\mathbf{u}}\;\mathbf{u}. \tag{3}$$

Note that the roller's rotation around $\mathbf{n}_\gamma$ giving rise to the first term on the right-hand side of (3) is completely passive, whereas the wheel rotation around $\mathbf{n}$ giving rise to the second term on the right-hand side of (3) is assumed to be actively produced by a motor. Calling $\mathbf{n}_h\;\dot{q}_h$ the angular speed associated with the hth motor in the body-fixed frame, in case of perfect rolling, the mapping between the "joint" speed $\dot{q}$ and the corresponding velocity $\mathbf{v}$ of the hub of any given wheel will be given by

$$\frac{\mathbf{n}_\gamma^T}{\mathbf{u}^T\mathbf{n}_\gamma}\;\mathbf{v} = \rho\,\dot{q} \tag{4}$$

where the contribution

$$\frac{\mathbf{n}^T\mathbf{v}}{\mathbf{u}_\gamma^T\mathbf{n}}\;\mathbf{u}_\gamma^T\;\mathbf{u}$$

of $\mathbf{v}$ in direction of $\mathbf{u}$ has been explicitly assumed *not* to contribute to $\rho\,\dot{q}$, as in the given hypothesis of perfect rolling, it is fully generated by the passive rotation of the roller. Substituting (2) back into (4), given that $\mathbf{u}_h^T\,\mathbf{n}_{\gamma h} = -\cos\gamma$ for any h, one gets

$$-\frac{1}{\cos\gamma}\,\mathbf{n}_{\gamma h}^T\;\mathbf{v}_c + \frac{1}{\cos\gamma}\,\mathbf{n}_{\gamma h}^T\;S(\mathbf{b}_h)\,\mathbf{k}\,\omega = \rho\,\dot{q}_h\,. \tag{5}$$

By projecting all the vectors in (5) on a common body-fixed frame with its third axis equal to $\mathbf{k} \perp \mathcal{P}$, the term $\mathbf{n}_{\gamma h}^T\;S(\mathbf{b}_h)\,\mathbf{k}$ results in

$$\mathbf{n}_{\gamma h}^T\;S(\mathbf{b}_h)\,\mathbf{k} = n_{\gamma x h}\;b_{yh} - n_{\gamma y h}\;b_{xh} = -\mathbf{b}_h^T\;\mathbf{u}_{\gamma h}\,. \tag{6}$$

Summarizing, (5) can be interpreted as a generic component of the inverse differential kinematics equation in matrix form

$$M\begin{pmatrix}\mathbf{v}_c\\ \omega\end{pmatrix} = \rho\,\dot{\mathbf{q}}\,\cos\gamma \tag{7}$$

where

$$M = -\begin{pmatrix} n_{\gamma x 1} & n_{\gamma y 1} & \mathbf{b}_1^T\;\mathbf{u}_{\gamma 1}\\ n_{\gamma x 2} & n_{\gamma y 2} & \mathbf{b}_2^T\;\mathbf{u}_{\gamma 2}\\ \vdots & \vdots & \vdots\\ n_{\gamma x N} & n_{\gamma y N} & \mathbf{b}_N^T\;\mathbf{u}_{\gamma N}\end{pmatrix} \in \mathbb{R}^{N\times 3} \tag{8}$$

and $\dot{\mathbf{q}} \in \mathbb{R}^{N\times 1}$ is the vector of joint velocities. Equations (7) and (8) represent the general kinematics model [9] of a Swedish wheeled vehicle with N wheels. Contrary to most of the other models presented in the literature that are relative to three or four wheels in fixed configurations, they allow a fully detailed analysis of the vehicle kinematics properties as a function of not only the roller–wheel hub orientation γ, but also the relative wheel position. Such an analysis may be extremely useful for the mechanical and controls system design of the vehicle.

Assuming $\cos\gamma \neq 0$ and that M has rank 3, equation (7) can be used to compute joint velocity commands for a desired vehicle speed $(\mathbf{v}_{cd}^T, \omega_d)^T$. In particular, the following lemma holds.

Lemma 1: Given a Swedish wheeled mobile robot with N identical wheels of radius ρ satisfying (7), any desired vehicle velocity $(\mathbf{v}_{cd}^T, \omega_d)^T$ can be implemented by using proper joint velocities $\dot{\mathbf{q}}_d$ if and only if all of the following conditions hold:

c.1 $\cos\gamma \neq 0$;

c.2 rank $M = 3$.

In particular,

$$\dot{\mathbf{q}}_d = \frac{1}{\rho\,\cos\gamma}\,M\begin{pmatrix}\mathbf{v}_{cd}\\ \omega_d\end{pmatrix}. \tag{9}$$

The violation of any of the previous conditions $c.1$ or $c.2$ corresponds to kinematics singularities of a different kind: the violation of condition $c.1$ would correspond to a total loss of control authority, while the violation of condition $c.2$ would correspond to a loss of controllability, as for any choice of the input $\dot{\mathbf{q}}$, the state derivative $(\mathbf{v}_c^T, \omega)^T$ would not be uniquely defined.

Matrix M defined in (8) can be decomposed as $M = [M_l\;M_a]$, where $M_l \in \mathbb{R}^{N\times 2}$ and $M_a \in \mathbb{R}^{N\times 1}$ such that

$$M_l\,\mathbf{v}_c + M_a\,\omega = \rho\,\dot{\mathbf{q}}\,\cos\gamma. \tag{10}$$

III. Guidance Control of Swedish Wheeled Omnidirectional Robots

Based on the derived kinematical model, the trajectory tracking and pose regulation motion control problems for a generic robot equipped with $N \geq 3$ Swedish wheels are solved. The proposed solution, besides being general in terms of number of wheels, value of γ, and wheel configuration, explicitly accounts for joint velocity saturation. The control problem is formulated as a *guidance control* problem, namely the joint velocities $\dot{q}_h$ are assumed to be control inputs and the robots linear and angular velocities $\mathbf{v}_c$ and ω satisfying (7) are the outputs. Of course, in practice, such an approach requires the implementation of a lower level control loop mapping the joint reference speeds $\dot{\mathbf{q}}_d$ in actuator commands.

A. Low-Level Control Design

As in standard robot motion control architectures [22], the low-level control system can be designed either in a decentralized or in a centralized fashion. In the former case, each actuator is controlled separately, typically with a velocity PID loop (as for the experimental validation reported in this paper); in the latter case, a centralized control solution can be derived based on computed torque (i.e., feedback linearization) methods.

The decentralized control (or independent joint control) method is simpler: each component of $\dot{\mathbf{q}}_d$ is used as a reference signal for the corresponding PID actuator velocity loop, and dynamic couplings among the actuators are neglected. If such low-level control system (i.e., each actuator velocity servo loop) is fast with respect to the robot dynamic-navigation one, the lag between the desired joint velocities and the real joint velocities is negligible: in such a case, as long as the perfect rolling constraint is satisfied, the mapping between the vehicle's velocity $(\mathbf{v}_c^T, \omega)^T$ and the joint speeds would be approximated by the system's kinematical model (7) having the *desired* (or commanded) joint velocities $\dot{\mathbf{q}}_d$ on the right-hand side in place of the real joint velocities $\dot{\mathbf{q}}$.

Centralized control solutions are generally based on the dynamic robot model [17, Ch. 12, pp. 493–502], and the dynamic equation of Swedish wheeled robots with a geometry as the one described in Section II has the following structure:

$$I\,\ddot{\mathbf{q}} + (C(\omega) + F)\,\dot{\mathbf{q}} = \boldsymbol{\tau} \tag{11}$$

with $I \in \mathbb{R}^{N\times N}$ being the positive-definite inertia matrix, $C(\omega) \in \mathbb{R}^{N\times N}$ the skew-symmetric Coriolis and centrifugal forces matrix ($\omega\mathbf{k}$ is the robot's angular velocity), $F \in \mathbb{R}^{N\times N}$ the diagonal friction matrix, and $\boldsymbol{\tau} \in \mathbb{R}^{N\times 1}$ the actuator torque's vector. Given the nondiagonal nature of matrices I and $C(\omega)$ and the dependency (7) of ω from $\dot{\mathbf{q}}$, (11) is nonlinear and coupled. Yet, as commonly done for robotic manipulators [22], the control input vector $\boldsymbol{\tau}$ can be computed based upon a nonlinear state feedback linearization (or computed torque) solution, namely

$$\boldsymbol{\tau} = (C(\omega) + F)\,\dot{\mathbf{q}} + I\,\mathbf{y} \tag{12}$$

giving rise (recall that I is full rank) to a linear and decoupled model

$$\ddot{\mathbf{q}} = \mathbf{y}$$

that can then be used to design a closed-loop solution for $\mathbf{y}$ in order to track the reference signal $\dot{\mathbf{q}}_d$.

Given that the computed torque solution explicitly accounts for the system's dynamic coupling terms, it is expected to exhibit a better tracking performance, in particular, for high speed and acceleration references. Nevertheless, as also demonstrated by the reported experimental results, the independent joint solution appears to be sufficiently precise and accurate for tracking simple trajectories at constant speed. Moreover, given that the main objective of this research was to validate an actuator velocity management strategy at the guidance level, only the independent joint low-level control solution (i.e., actuator PID velocity servo loop) was implemented.

In the following, the Swedish wheeled robot will be assumed to have such kind of low-level independent joint controls system, and the trajectory tracking and pose regulation problems will be solved at the guidance level, i.e., considering the commanded joint speeds $\dot{\mathbf{q}}_d$ as control inputs and $(\mathbf{v}_c^T, \omega)^T$ as outputs according to the purely kinematical model (10). In order to formulate the trajectory tracking and pose regulation problems, the following notation will be used: given an inertial (global) frame $\langle G\rangle = (\mathbf{i}, \mathbf{j}, \mathbf{k})$ with $\mathbf{k} := (\mathbf{i} \times \mathbf{j}) \perp \mathcal{P}$, where $\mathcal{P}$ is the floor plane, a reference (planar) trajectory is a differentiable curve in $\mathcal{P}$

$$\mathbf{r}_d(t) = \mathbf{i}\,\left(\mathbf{r}_d^T(t)\mathbf{i}\right) + \mathbf{j}\,\left(\mathbf{r}_d^T(t)\mathbf{j}\right) \tag{13}$$

with curvilinear abscissa

$$s(t) := \int_{t_0}^{t} \left\| \frac{d\,\mathbf{r}_d(\tau)}{d\tau} \right\| d\tau \tag{14}$$

and unit tangent vector

$$\mathbf{t}_d = \frac{d\,\mathbf{r}_d}{ds}. \tag{15}$$

The kinematics trajectory tracking problem consists in finding a control law for the system's input $\dot{\mathbf{q}}_d$ such that the position and heading tracking errors

$$\mathbf{e}_r(t) := \mathbf{r}_d(t) - \mathbf{r}_c(t) \tag{16}$$

$$e_\varphi(t) := \varphi_d(t) - \varphi(t) \tag{17}$$

converge to zero, with $\mathbf{r}_c(t)$ being the position in $\langle G\rangle$ of a reference point (e.g., the geometrical center or the center of mass) of the robot, $\varphi(t)$ its heading, and $\varphi_d(t)$ the desired reference heading. Note that for nonholonomic vehicles having a unicycle or car-like kinematics model, the reference heading $\varphi_d(t)$ is *not* arbitrary, but needs to coincide with the heading of the trajectories unit tangent vector $\mathbf{t}_d$. Conversely, given any position reference trajectory $\mathbf{r}_d(t)$, a Swedish wheeled vehicle will be free to track any arbitrary heading $\varphi_d(t)$ that does not necessarily need to coincide with the heading of $\mathbf{t}_d$.

The pose regulation problem is a special case of the trajectory tracking one occurring when the position and orientation references are constant, i.e., when $\dot{\mathbf{r}}_d = \mathbf{0}$ and $\dot{\varphi}_d = 0$.

B. Trajectory Tracking Controller Design

In accordance with the notation previously introduced, consider the system in (10) with $\dot{\mathbf{r}}_c(t) = \mathbf{v}_c$ and $\dot{\varphi}(t) = \omega$ being the robots linear and angular velocities. Assuming that conditions $c.1$ and $c.2$ of Lemma 1 are satisfied, $N \geq 3$, and $M_a \perp \text{span}(M_l)$ (this can be always guaranteed by a proper design of the robot geometry), then any desired robot linear velocity $\mathbf{v}_c = (\cdot, \cdot, 0)^T$ and angular velocity $\omega\,\mathbf{k}$ are uniquely mapped to the control input $\dot{\mathbf{q}}_d$ as follows:

$$\dot{\mathbf{q}}_d = \dot{\mathbf{q}}_{dl} + \dot{\mathbf{q}}_{da} \tag{18}$$

$$\dot{\mathbf{q}}_{dl} = \frac{1}{\rho\cos\gamma}\,M_l\,\mathbf{v}_c \tag{19}$$

$$\dot{\mathbf{q}}_{da} = \frac{1}{\rho\cos\gamma}\,M_a\,\omega. \tag{20}$$

Following a standard approach, to solve the trajectory tracking problem, consider the Lyapunov candidate function

$$V = \frac{1}{2}\mathbf{e}_r^T\, K_r\, \mathbf{e}_r + \frac{1}{2}e_\varphi^T\, K_\varphi\, e_\varphi \tag{21}$$

with $K_r \in \mathbb{R}^{2\times 2}$ being a symmetric positive definite ($K_r > 0$) matrix and K_φ a positive constant. The time derivative of V results in

$$\dot{V} = \mathbf{e}_r^T\, K_r\, (\dot{\mathbf{r}}_d(t) - \mathbf{v}_c) + e_\varphi^T\, K_\varphi\, (\dot{\varphi}_d(t) - \omega)\,. \tag{22}$$

If $\mathbf{v}_c$ and ω satisfy

$$\mathbf{v}_c = \dot{\mathbf{r}}_d(t) + K_r\, (\mathbf{r}_d(t) - \mathbf{r}_c(t)) \tag{23}$$

$$\omega = \dot{\varphi}_d(t) + K_\varphi\, (\varphi_d(t) - \varphi(t)) \tag{24}$$

then the time derivative of V will be negative definite, i.e.

$$\dot{V} = -\mathbf{e}_r^T\, K_r\, K_r\, \mathbf{e}_r - (K_\varphi\, e_\varphi)^2 < 0. \tag{25}$$

Substituting (23) and (24) in (19) and (20), the corresponding joint velocity command results in

$$\dot{\mathbf{q}}_d(t) = \dot{\mathbf{q}}_{dl}(t)\ +\ \dot{\mathbf{q}}_{da}(t) \tag{26}$$

$$\dot{\mathbf{q}}_{dl}(t) = \frac{1}{\rho\cos\gamma}\, M_l\, \dot{\mathbf{r}}_d(t) + \frac{1}{\rho\cos\gamma}\, M_l\, K_r\, (\mathbf{r}_d(t) - \mathbf{r}_c(t)) \tag{27}$$

$$\dot{\mathbf{q}}_{da}(t) = \frac{1}{\rho\cos\gamma}\, M_a\, \dot{\varphi}_d(t) + \frac{1}{\rho\cos\gamma}\, M_a\, K_\varphi\, (\varphi_d(t) - \varphi(t))\,. \tag{28}$$

The solution in (26) is a combination of feedforward terms proportional to the reference linear and angular velocities and a feedback term proportional to the tracking error. The proposed solution guarantees global exponential stability of equilibrium $\mathbf{e}_r = \mathbf{0}, e_\varphi = 0$ of the error dynamics, thus (robustly) solving the trajectory tracking problem. Control law (26) is the sum of two contributions: the first (27) relative to position tracking and the second (28) to heading tracking. It should be noted that due to the hypothesis that $M_a \perp \text{span}(M_l)$, the two commands (27) and (28) do not interfere with each other, namely the contribution of $\dot{\mathbf{q}}_{dl}$ to the robot's angular velocity and the contribution of $\dot{\mathbf{q}}_{da}$ to the robot's linear velocity are both null.

C. Actuator Saturation Issues

The aforementioned analysis of the derived control law implicitly assumes that the robot can actually (and instantly) implement any $\dot{\mathbf{q}}_d$ no matter its norm. In practice, actuators will not be ideal: in particular, they will have a nonnull response time and an upper bound on the maximum output. As far as the time response is concerned, it must be assumed that the lower level actuator velocity servo loop is much faster than the guidance (kinematics) loop. This requirement is reflected on design choices as actuator power and reference trajectories: the former needs to be sufficiently large for the given inertial properties of the vehicle so that maximum vehicle accelerations can be much larger than the maximum reference accelerations $\ddot{\varphi}_d(t)$ and $\ddot{\mathbf{r}}_d(t)$. As far as the ratio of maximum vehicle acceleration over maximum reference acceleration is sufficiently large, the dynamic behavior of the kinematics guidance law will be fine. Thus, as for any other kinematics-designed guidance solution, the proposed control law should be implemented on Swedish wheeled vehicles with sufficiently powerful actuators with respect to the maximum reference accelerations $\ddot{\varphi}_d(t)$ and $\ddot{\mathbf{r}}_d(t)$. Should one decide to tackle wheel slipping and skidding phenomena [15], [19] by designing motion controllers based on the dynamical model (11) of the robot, a lower level control loop [dynamics based as sketched by (12)] should be added to the kinematics-based guidance loop (as suggested in [16]). For a discussion about dynamical models of mobile robots equipped with Swedish wheels, refer to [17] or [13] and [18], where such a model is employed to compute near-optimal trajectories. As for actuator velocity saturation, the situation is slightly more complex. Given the proportional nature of the control law (26), the tracking error (either in position or heading) or the desired reference velocities can always happen to be large enough for the actuators to reach their limits. Calling $\dot{q}_{\max j} > 0$, the absolute value of the maximum possible velocity of actuator j, a threshold for $\|\dot{\mathbf{q}}_d\|_\infty$ can be selected as $\dot{q}_{\max} = \min_j \{\dot{q}_{\max j}\}$, where $j = 1, 2, \ldots, N$. Whatever the gains K_r and K_φ, depending on $\dot{\varphi}_d(t)$, $\dot{\mathbf{r}}_d(t)$, $\mathbf{e}_r(t)$, or $e_\varphi(t)$, the saturation condition

$$\|\dot{\mathbf{q}}_d\|_\infty\ \le\ \dot{q}_{\max} \tag{29}$$

may always be violated. Note that while the feedforward signals $\dot{\varphi}_d(t)$ and $\dot{\mathbf{r}}_d(t)$ can eventually always be bounded, the tracking error's initial conditions are not design parameters. Hence, a commanded $\dot{\mathbf{q}}_d$ with an exceeding infinity norm due to odd initial conditions cannot be *a priori* excluded.

D. Tracking in Presence of Actuator Velocity Saturation

The presence of actuator velocity saturation has a severe impact on performance: in particular, given the additive structure of (26), actuator velocity saturation can affect the decoupling between commanded angular and linear vehicle velocities in spite of the fact that M_a does not belong to the span of M_l. With reference to (26), suppose, for example, that all the components of $\dot{\mathbf{q}}_{dl}(t)$ are within the actuator limits, but that as a consequence of adding $\dot{\mathbf{q}}_{da}(t)$, some of the overall commanded joint speeds $\dot{\mathbf{q}}_d(t)$ exceed the actuator limits. In this case, both the robot-commanded linear and angular velocities will be corrupted in an unpredictable fashion. A (known) quick and dirty way out of this problem could be to simply scale down $\dot{\mathbf{q}}_d(t)$ such that all its components are within acceptable bounds. This, of course, will always guarantee that the commanded joint speeds are within the proper bounds, but one would need to prove that such a strategy does not jeopardize the asymptotic stability of the tracking error to zero. Moreover, in many applications, it may happen that either linear or angular velocity commands may have highest priority. In such a case, scaling down the overall joint commands will have a negative effect of slowing down the convergence speed of the highest priority task due to the presence of the lower priority one. In order to cope with this and to guarantee a prioritized execution of the position and heading tracking tasks, the following modification of the proposed control law is suggested: the sum in (26) should be weighted with error- and reference-dependent weights such that: 1) the resulting $\dot{\mathbf{q}}_d$ command has norm within the actuator limits; 2) the tasks (position and heading tracking in the present case) are executed with a priority-based time order (higher priority tasks first); and 3) the tracking error converges to zero.

Consider the saturation function

$$\sigma : \mathbb{R} \times [0, \infty) \longrightarrow \mathbb{R}$$

$$\sigma(x, c) = \begin{cases} 0, & \text{if}\quad x = 0 \\ 1, & \text{if}\quad 0 < |x| < c \\ c/|x|, & \text{otherwise.} \end{cases} \tag{30}$$

In the following, the nonnegative second argument c of $\sigma(x, c)$ will be called the capacity of x. Note that by definition, $\sigma(x, c)$ is simply a nonnegative scalar scaling factor such that $x\,\sigma(x, c)$ is "clipped" to $c\,\text{sign}(x)$ whenever $|x|$ should exceed the capacity c and is equal to

x otherwise, i.e., $x\,\sigma(x,c)$ is simply the saturated version of x in the range $[-c,c]$. Also note that by its very definition

$$\sigma(x,0)=0 \qquad \forall\, x \tag{31}$$

namely if x should be assigned zero capacity, then $x\,\sigma(x,0)=0$ for any value of x. Assume that

$$\dot{\mathbf{q}}_d=\sum_{h=1}^{n}\dot{\mathbf{q}}_h \tag{32}$$

is the actuator input with $\dot{\mathbf{q}}_1,\dot{\mathbf{q}}_2,\ldots,\dot{\mathbf{q}}_n$ n independent task inputs ordered by decreasing priority with increasing index ($\dot{\mathbf{q}}_1$ has highest priority). Each term on the right-hand side of (32) and $\dot{\mathbf{q}}_d$ itself should have infinity norm bounded by $\dot{q}_{\max}$. Considering that each task should be executed in a prioritized fashion, the sum in (32) may be replaced by a weighted sum as follows:

$$\begin{aligned}\dot{\mathbf{q}}_d=&\,\dot{\mathbf{q}}_1\,\sigma\left(\|\dot{\mathbf{q}}_1\|_\infty,c_1\right)\\&+\dot{\mathbf{q}}_2\,\sigma\left(\|\dot{\mathbf{q}}_2\|_\infty,c_2\right)\\&+\;\vdots\\&+\dot{\mathbf{q}}_n\,\sigma\left(\|\dot{\mathbf{q}}_n\|_\infty,c_n\right)\end{aligned} \tag{33}$$

where each task capacity is recursively and dynamically computed as

$$\begin{aligned}&c_1(t)\le\dot{q}_{\max}\quad\text{(positive constant, i.e., }\dot{c}_1(t)=0)\\&c_2(t)=c_1-\|\dot{\mathbf{q}}_1\|_\infty\,\sigma\left(\|\dot{\mathbf{q}}_1\|_\infty,c_1\right)\\&c_3(t)=c_2(t)-\|\dot{\mathbf{q}}_2\|_\infty\,\sigma\left(\|\dot{\mathbf{q}}_2\|_\infty,c_2(t)\right)\\&\quad\vdots=\vdots\\&c_n(t)=c_{n-1}(t)-\|\dot{\mathbf{q}}_{n-1}\|_\infty\,\sigma\left(\|\dot{\mathbf{q}}_{n-1}\|_\infty,c_{n-1}(t)\right).\end{aligned} \tag{34}$$

Note that, by construction, all the previous task capacities are nonnegative, i.e.

$$c_j\ge 0 \qquad \forall\, j\in[1,n]$$

and that

$$\begin{aligned}&c_j\;\le\;c_{j-1} \qquad \forall\, j\in[2,n]\\&c_i=0\implies c_j=0 \qquad \forall\, j>i\end{aligned}$$

namely if a given task is assigned zero capacity, all the lower priority tasks will also automatically have zero capacity and all their weights in the sum (33) will be zero. The capacity of task i can be viewed as the residual capacity after the higher priority task $i-1$ has been commanded; thus, for example, c_2 will be zero (and also $c_j:j>2$) if the task 1 input $\dot{\mathbf{q}}_1$ is saturating all its capacity c_1. In other words, each task will be commanded with a nonnull weight only if the higher priority tasks have not saturated. The fact that c_1 should not exceed $\dot{q}_{\max}$ is due to the fact that task 1 alone should not saturate the actuator capacity $\dot{q}_{\max}$; moreover, given that $c_{j+1}\le c_j\ \forall\, j\in[1,n-1]$, the condition $c_1\le\dot{q}_{\max}$ guarantees that *each* term in the sum (33) will have infinity norm smaller or equal to the threshold $\dot{q}_{\max}$. A proof that (33) and (34) also imply

$$\|\dot{\mathbf{q}}_d\|_\infty=\left\|\sum_{h=1}^{n}\dot{\mathbf{q}}_h\,\sigma\left(\|\dot{\mathbf{q}}_h\|_\infty,c_h\right)\right\|_\infty\;\le\;\dot{q}_{\max} \tag{35}$$

is reported in the Appendix. In order to implement the aforementioned described schema in the present trajectory tracking case, assume that the reference feedforward linear and angular velocities are sufficiently small, namely that

$$\frac{1}{\rho|\cos\gamma|}\;\|M_l\,\dot{\mathbf{r}}_d(t)\|_\infty\;<\;\frac{1}{2}\;\dot{q}_{\max}\qquad\forall\, t \tag{36}$$

$$\frac{1}{\rho|\cos\gamma|}\;\|M_a\,\dot{\varphi}_d(t)\|_\infty\;<\;\frac{1}{2}\;\dot{q}_{\max}\qquad\forall\, t. \tag{37}$$

These conditions are necessary to guarantee that the tracking task is asymptotically feasible, namely that when the position and heading tracking errors are null, the control effort of the control law (26) is compatible with the actuator velocity saturation limit, i.e.

$$\begin{aligned}&\mathbf{e}_r=\mathbf{0},e_\varphi=0\Longrightarrow\\&\quad\|\dot{\mathbf{q}}_d(t)\|_\infty=\frac{1}{\rho|\cos\gamma|}\;\|M_l\,\dot{\mathbf{r}}_d(t)+M_a\,\dot{\varphi}_d(t)\|_\infty\\&\quad\le\frac{1}{\rho|\cos\gamma|}\;\left[\|M_l\,\dot{\mathbf{r}}_d(t)\|_\infty+\|M_a\,\dot{\varphi}_d(t)\|_\infty\right]<\dot{q}_{\max}.\end{aligned}$$

For the sake of clarity, assume that position tracking is assigned highest priority with respect to heading tracking. The following are defined:

$$\dot{\mathbf{q}}_1:=\frac{1}{\rho\cos\gamma}\,M_l\,\dot{\mathbf{r}}_d(t) \tag{38}$$

$$\dot{\mathbf{q}}_2:=\frac{1}{\rho\cos\gamma}\,M_l\,K_r\,\left(\left(\mathbf{r}_d(t)-\mathbf{r}_c(t)\right)\right. \tag{39}$$

$$\dot{\mathbf{q}}_3:=\frac{1}{\rho\cos\gamma}\,M_a\,\dot{\varphi}_d(t) \tag{40}$$

$$\dot{\mathbf{q}}_4:=\frac{1}{\rho\cos\gamma}\,M_a\,K_\varphi\,\left(\varphi_d(t)-\varphi(t)\right). \tag{41}$$

With these definitions, consider the control law (33) and (34) with

$$c_1(t)=\dot{q}_{\max}\;>\;0\qquad\forall\, t$$

that together with the feasibility condition (36) implies

$$0\;<\;\frac{1}{2}\,\dot{q}_{\max}\;\;\le\;\;c_2\;\;\le\;\;\dot{q}_{\max}$$

i.e., the tasks 1 and 2 always have nonnull capacity. Moreover, by hypothesis $\|\dot{\mathbf{q}}_1\|_\infty<0.5\,\dot{q}_{\max}$ [see (36)] and $c_1=\dot{q}_{\max}$, it follows that

$$\dot{\mathbf{q}}_1\,\sigma(\|\dot{\mathbf{q}}_1\|_\infty,c_1)=\dot{\mathbf{q}}_1\qquad\forall\, t.$$

This fact together with the assumption that $M_a\perp\text{span}(M_l)$ implies that by substituting (38)–(41) in (33) and (34), the vehicle will have linear and angular velocities given by

$$\mathbf{v}_c(t)=\dot{\mathbf{r}}_d(t)+K_r\,\mathbf{e}_r(t)\,\sigma(\|\dot{\mathbf{q}}_2\|_\infty,c_2) \tag{42}$$

$$\omega(t)=\dot{\varphi}_d(t)\,\sigma(\|\dot{\mathbf{q}}_3\|_\infty,c_3)+K_\varphi\,e_\varphi(t)\,\sigma(\|\dot{\mathbf{q}}_4\|_\infty,c_4). \tag{43}$$

Note that the term $\sigma(\|\dot{\mathbf{q}}_2\|_\infty,c_2)$ will be zero if and only if $\|\dot{\mathbf{q}}_2\|_\infty=0$ due to the fact that c_2 is strictly positive. Consequently

$$\begin{aligned}&V_1=\frac{1}{2}\mathbf{e}_r^T\,K_r\,\mathbf{e}_r\quad\Longrightarrow\\&\dot{V}_1=\mathbf{e}_r^T\,K_r\,\left(\dot{\mathbf{r}}_d(t)-\mathbf{v}_c(t)\right)\\&\quad=-\mathbf{e}_r^T\,K_r\,K_r\,\mathbf{e}_r(t)\,\sigma(\|\dot{\mathbf{q}}_2\|_\infty,c_2)<0\end{aligned} \tag{44}$$

i.e., $\dot{V}_1$ is negative definite thus proving asymptotic global Lyapunov stability of $\mathbf{e}_r=\mathbf{0}$. Note that $\dot{\mathbf{q}}_3$ and $\dot{\mathbf{q}}_4$ do not contribute to $\dot{V}_1$ as they

belong to the range of M_a that is normal to the span of M_l. As far as the secondary (heading) task is concerned, convergence can also be proven through a Lyapunov argument. The global asymptotic stability of $\mathbf{e}_r = \mathbf{0}$ guarantees that

$$\lim_{t\to\infty} \dot{\mathbf{q}}_2(t) = \mathbf{0} \quad \Longrightarrow \quad \lim_{t\to\infty} c_3 = c_2 \;\geq\; \frac{1}{2}\dot{q}_{\max}.$$

Given the feasibility condition (37), this means that

$$\exists\ t^* \ :\ \dot{\mathbf{q}}_3\,\sigma(\|\dot{\mathbf{q}}_3\|_\infty, c_3) = \dot{\mathbf{q}}_3 \qquad \text{and} \qquad c_4 > 0 \qquad \forall\, t \geq t^*$$

implying

$$\omega(t)|_{t\geq t^*} = \dot{\varphi}_d(t) + K_\varphi\, e_\varphi(t)\,\sigma(\|\dot{\mathbf{q}}_4\|_\infty, c_4) \tag{45}$$

where $\sigma(\|\dot{\mathbf{q}}_4\|_\infty, c_4)$ is zero if and only if $\|\dot{\mathbf{q}}_4\|_\infty = 0$ due to the fact that c_4 is strictly positive for $t \geq t^*$. Consequently

$$\begin{aligned} V_2 &= \frac{1}{2} e_\varphi^T\, K_\varphi\, e_\varphi \quad \Longrightarrow \\ \dot{V}_2(t)\Big|_{t\geq t^*} &= e_\varphi^T\, K_\varphi\, \left(\dot{\varphi}_d(t) - \omega(t)\right) \\ &= -e_\varphi^T\, K_\varphi^2\, e_\varphi(t)\,\sigma\left(\|\dot{\mathbf{q}}_4\|_\infty, c_4\right) < 0 \end{aligned} \tag{46}$$

namely there exists a finite time t^* after which the time derivative of V_2 is always negative, thus proving convergence to zero of the heading error $e_\varphi(t)$. Prior to t^*, the heading (secondary task) error $e_\varphi(t)$ is not guaranteed to be decreasing. Note that $\dot{\mathbf{q}}_1$ and $\dot{\mathbf{q}}_2$, being in the range of M_l and normal to M_a, do not contribute to $\dot{V}_2$.

In case the heading should be selected to be the highest priority task, it would be sufficient to select $\dot{\mathbf{q}}_1, \ldots, \dot{\mathbf{q}}_4$ as

$$\dot{\mathbf{q}}_1 := \frac{1}{\rho\cos\gamma}\, M_a\, \dot{\varphi}_d(t) \tag{47}$$

$$\dot{\mathbf{q}}_2 := \frac{1}{\rho\cos\gamma}\, M_a\, K_\varphi\, e_\varphi \tag{48}$$

$$\dot{\mathbf{q}}_3 := \frac{1}{\rho\cos\gamma}\, M_l\, \dot{\mathbf{r}}_d(t) \tag{49}$$

$$\dot{\mathbf{q}}_4 := \frac{1}{\rho\cos\gamma}\, M_l\, K_r\, \mathbf{e}_r(t) \tag{50}$$

in (33) and (34); Lyapunov stability of the heading error and asymptotic convergence of the position error could be proven accordingly.

As for constant pose control, the trajectory tracking problem is reduced to a pose (position and orientation) regulation one as soon as the reference position and heading trajectories $\mathbf{r}_d(t)$ and $\varphi_d(t)$ are constant.

IV. Experimental Validation

The described guidance law for trajectory tracking in the presence of actuator velocity saturation has been experimentally validated on a three Swedish wheel robot with $\gamma = 0^\circ$ and $\rho = 5$ cm [20], [21]. The robot, named Volksbot, has been designed and built at the Fraunhofer Autonomous Intelligent Systems Institute (AiS)[1] of Sankt Augustin, Germany. The vehicle's geometry depicted in Fig. 3 is such that $\|\mathbf{b}_i\| = \|\mathbf{b}_j\| = 25$ cm for all i, j. This implies that $M_a \perp \text{span}(M_l)$.

The platform is actuated by three 24 V dc motors of 90 W each with 1:8 gear ratio and is about 8 kg in weight. Optical encoders are mounted on each motor shaft to provide feedback for the motor speed regulator. The controls system architecture is rather standard: it has an external kinematics loop closed on the low-level actuator velocity servo loops. In particular, the low-level motor speed feedback control is realized by a three-channel digital PID board (the TMC200 designed and built at AiS) with pulsewidth modulation (PWM) output. The maximum

[1]Ais has now merged with another Fraunhofer Institute giving rise to the new Fraunhofer Institute for Intelligent Analysis and Information Systems (IAIS).

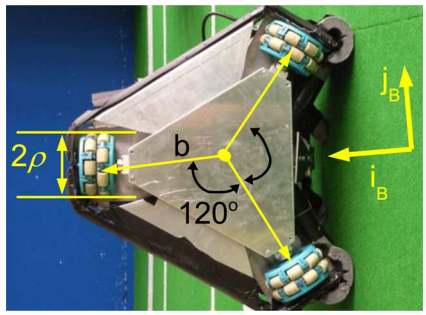

Fig. 3. Geometrical model of the Volksbot robot used for experimental validation of the trajectory tracking control law.

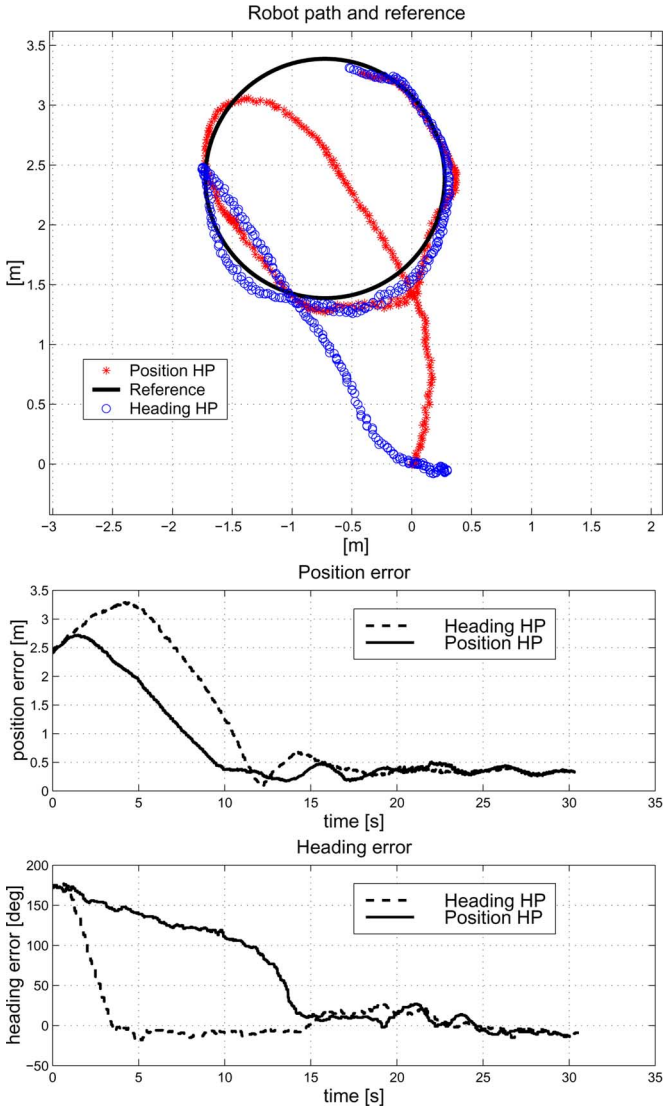

Fig. 4. Experimental results: driven paths and tracking errors. The highest priority task is shown to always converge faster in spite of the fact that the lower priority ones causes actuator velocity saturation.

continuous current provided to each motor by the TMC200 board is 8 A with the peak value being 20 A. The TMC200 board is interfaced through a serial RS232 link with an onboard laptop PC implementing the guidance and navigation systems. The navigation system providing the estimates of the robot poses used to close the guidance control loop is based on the integration of odometry and an omnidirectional vision system. This builds on a 30-Hz, 640 × 480 pixels YUV color FireWire camera pointing toward a 70-mm-diameter hyperbolic mirror.

In order to validate the performance of the designed trajectory tracking control law, a reliable measurement of the robot's pose is mandatory. To this extent, an experimental setup was designed at AiS where the position of the robot was measured by a fixed laser range finder pointing toward the robot. The robot's heading, instead, was evaluated based on the onboard omnidirectional vision system. The reference position and heading to be tracked and all the collected data were suitably synchronized. Examples of the experimental results are reported in Fig. 4: the position reference was a circular trajectory having radius of 1 m while the heading reference was constant (with respect to a fixed frame). The reported results refer to the cases where either heading (47)–(50) or position (38)–(41) tracking was the task with high priority (HP). The reference trajectory was designed so to satisfy the feasibility conditions (36) and (37), and the robot's initial conditions were specifically chosen to be large enough to trigger actuator velocity saturation: due to experimental setup constraints, the actuators were artificially forced to saturate at ±8.7 rad/s via low-level control software (corresponding to maximum robot linear and angular velocities of about 0.5 m/s and 99.7°/s respectively). As expected, both heading and position errors are always asymptotically converging to zero (besides measuring errors visible in the error plots), but the task with HP always converges first. Note that the position errors are increasing (also when position tracking has highest priority) in the very first few seconds of the experiment as a consequence of the neglected dynamics of the vehicle.

V. Conclusion

A general kinematics model of an N Swedish wheeled vehicle was derived and analyzed. Having addressed the N Swedish wheel case, the provided results allow to unify the analysis of the common three- and four-wheel designs that are usually performed separately. Moreover, the derived analysis can be immediately and simply applied to explore, for example, eventual six-wheel designs for outdoor and rough terrain applications or steering (i.e., with variable orientation) wheel designs, as in [12], that allow the implementation of continuously variable transmission (CVT) systems.

The trajectory tracking motion control problem in the presence of actuator velocity saturation has been addressed. Joint velocity saturation is always present and may heavily impact on the performance of motion control solutions. The originality and relevance of the proposed solution is related to the handling of the actuator velocity saturation constraints. The designed solution guarantees that each task joint velocity command and the overall commanded joint velocity have upper-bounded infinity norm compatible with each actuator limit. This is achieved by dynamically allocating control effort to the tasks according to their priority. Contrary to standard-task-based controllers, the presence of velocity saturations related to lower level tasks does not jeopardize the execution of higher priority ones. Global convergence of the tracking error has been theoretically proven and experimentally validated.

Future research will be devoted to the extension of the proposed saturation management technique in case of dynamic-based low-level control and to the generalization of the solution in case of multiple tasks in redundant robotic systems.

Acknowledgment

The author is deeply grateful to P. G. Plöger and J. Paulus of the Bonn Rhein Sieg University of Applied Science of Sankt Augusting, Germany for useful discussions and for having developed the setup for the experimental validation of the proposed control law. The author also thanks the anonymous reviewers for their comments.

Appendix

Proof of Statement 35

Proof: For the sake of notation compactness, define

$$\bar{\dot{q}}_j \stackrel{\text{def}}{=} \|\dot{\mathbf{q}}_j\|_\infty \, \sigma\left(\|\dot{\mathbf{q}}_j\|_\infty, c_j\right). \tag{51}$$

Then, summing the last $n-1$ equations (34) for $j = 2, 3, \ldots, n$, the following holds:

$$\sum_{j=2}^{n} c_j = c_1 + \sum_{l=2}^{n} c_l - c_n - \sum_{k=1}^{n-1} \bar{\dot{q}}_k \implies$$

$$c_1 = c_n + \sum_{k=1}^{n-1} \bar{\dot{q}}_k \geq \sum_{k=1}^{n} \bar{\dot{q}}_k \tag{52}$$

because $c_n \geq \bar{\dot{q}}_n$. Noticing that (33) implies

$$\|\dot{\mathbf{q}}_d\|_\infty \leq \sum_{h=1}^{n} \bar{\dot{q}}_h$$

(52) and the first of equations (34) imply

$$\|\dot{\mathbf{q}}_d\|_\infty \leq c_1 \leq \dot{q}_{\max}. \qquad \blacksquare$$

References

[1] O. Diegel, A. Badve, G. Bright, J. Potgieter, and S. Tlale, "Improved mecanum wheel design for omni-directional robots," presented at the Australian Conf. Robot. Autom., Auckland, New Zealand, Nov. 27–29, 2002.

[2] G. Campion, G. Bastin, and B. D'Andréa-Novel, "Structural properties and classification of kinematic and dynamic models of wheeled mobile robots," *IEEE Trans. Robot. Autom.*, vol. 12, no. 1, pp. 47–62, Feb. 1996.

[3] S. Ostrovskaya, "Dynamics of quasiholonomic and nonholonomic reconfigurable rolling robots," Ph.D. dissertation, Dept. Mech. Eng., McGill Univ., Montreal, QC, Canada, Jul. 2001.

[4] A. Salerno, S. Ostrovskaya, and J. Angeles, "The development of quasi-nonholonomic wheeled robots," in *Proc. 2002 IEEE Int. Conf. Robot. Autom. (ICRA 2002)*, Washington, DC, May, pp. 3514–3520.

[5] J. Agulló, S. Cardona, and J. Vivancos, "Kinematics of vehicles with directional sliding wheels," *Mech. Mach. Theory*, vol. 22, no. 4, pp. 295–301, 1987.

[6] P. F. Muir and C. P. Neuman, "Kinematic modeling for feedback control of an omnidirectional wheeled mobile robot," in *Autonomous Robot Vehicles*, J. Cox and G. T. Wilfong, Eds. New York: Springer-Verlag, 1990, pp. 25–31.

[7] F. G. Pin and S. M. Killough, "A new family of omnidirectional and holonomic wheeled platforms for mobile robots," *IEEE Trans. Robot. Autom.*, vol. 10, no. 4, pp. 480–489, Aug. 1994.

[8] H. Asama, M. Sato, L. Bogoni, H. Kaetsu, A. Matsumoto, and I. Endo, "Development of an omni-directional mobile robot with 3 DOF decoupling drive mechanism," in *Proc. 1995 IEEE Int. Conf. Robot. Autom. (ICRA 1995)*, Nagoya, Japan, pp. 1925–1930.

[9] S. K. Saha, J. Angeles, and J. Darcovich, "The design of kinematically isotropic rolling robots with omnidirectional wheels," *Mech. Mach. Theory*, vol. 30, no. 8, pp. 1127–1137, Nov. 1995.

[10] W. K. Loh, K. H. Low, and Y. P. Leow, "Mechatronics design and kinematic modelling of a singularityless omni-directional wheeled mobile robot," in *Proc. 2003 IEEE Int. Conf. Robot. Autom. (ICRA 2003)*, Tapei, Taiwan, Sep. 14–19, pp. 3237–3242.
[11] W. K. Kim, B.-J. Yi, and D. J. Lim, "Kinematic modeling of mobile robots by transfer method of augmented generalized coordinates," *J. Robot. Syst.*, vol. 21, no. 6, pp. 275–300, 2004.
[12] J.-B. Song and K.-S. Byun, "Design and control of a four-wheeled omnidirectional mobile robot with steerable omnidirectional wheels," *J. Robot. Syst.*, vol. 21, no. 4, pp. 193–208, 2004.
[13] O. Purwin and R. D'Andrea, "Trajectory generation and control for four wheeled omnidirectional vehicles," *Robot. Auton. Syst.*, vol. 54, no. 1, pp. 13–22, 2006.
[14] R. Volpe, J. Balaram, T. Ohm, and R. Ivlev, "The rocky 7 mars rover prototype," in *Proc. 1996 IEEE/RSJ Int. Conf. Intell. Robots Syst. (IROS 1996)*, Osaka, Japan, Nov. 4–8, vol. 3, pp. 1558–1564.
[15] R. L. Williams, II, B. E. Carter, P. Gallina, and G. Rosati, "Dynamic model with slip for wheeled omnidirectional robots," *IEEE Trans. Robot. Autom.*, vol. 18, no. 3, pp. 285–293, Jun. 2002.
[16] Y. Liu, J. J. Zhu, R. L. Williams, II, and J. Wu, "Omni-directional mobile robot controller based on trajectory linearization," *Robot. Auton. Syst.*, vol. 56, pp. 461–479, 2008.
[17] J. Angeles, *Fundamentals of Robotic Mechanical Systems*, 3rd ed. Berlin, Germany: Springer-Verlag, 2007.
[18] T. Kalmár-Nagy, R. D'Andrea, and P. Ganguly, "Near-optimal dynamic trajectory generation and control of an omnidirectional vehicle," *Robot. Auton. Syst.*, vol. 46, pp. 47–64, 2004.
[19] D. Wang and C. B. Low, "Modeling and analysis of skidding and slipping in wheeled mobile robots: Control design perspective," *IEEE Trans. Robot.*, vol. 24, no. 3, pp. 676–687, Jun. 2008.
[20] G. Indiveri, J. Paulus, and P. G. Plöger, "Task based kinematical robot control in the presence of actuator saturation and its application to trajectory tracking for an omniwheeled mobile robot," in *Proc. IEEE Int. Conf. Robot. Autom. (ICRA 2007)*, Rome, Italy, Apr. 10–14, pp. 2611–2616.
[21] G. Indiveri, J. Paulus, and P. G. Plöger, "Motion control of Swedish wheeled mobile robots in the presence of actuator saturation," in *RoboCup 2006: Robot Soccer World Cup X,* Lecture Notes in Computer Science, vol. 4437, Berlin, Heidelberg: Springer, 2007, pp. 35–46.
[22] L. Sciavicco and B. Siciliano, *Modelling and Control of Robot Manipulators*, 2nd ed. Berlin, Germany: Springer-Verlag, 2000.

Compliant Terrain Adaptation for Biped Humanoids Without Measuring Ground Surface and Contact Forces

Sang-Ho Hyon, *Member, IEEE*

***Abstract*—This paper reports the applicability of our passivity-based contact force control framework for biped humanoids. We experimentally demonstrate its adaptation to unknown rough terrain. Adaptation to uneven ground is achieved by optimally distributed antigravitational forces applied to preset contact points in a feedforward manner, even without explicitly measuring the external forces or the terrain shape. Adaptation to unknown inclination is also possible by combining an active balancing controller based on the center-of-mass (CoM) measurements with respect to the inertial frame. Furthermore, we show that a simple impedance controller for supporting the feet or hands allows the robot to adapt to low-friction ground without prior knowledge of the ground friction. This presentation includes supplementary experimental videos that show a full-sized biped humanoid robot balancing on uneven ground or time-varying inclination.**

***Index Terms*—Balance, compliance, contact force, humanoid robots, passivity-based control, redundancy, terrain adaptation.**

I. Introduction

Controlling force is the key technology for natural physical interaction for robots due to its causality to position and velocity. The recent expansion of assistive devices such as an exoskeletal system encourages better force control techniques to be investigated and integrative utilization for human–robot interaction. Such robotic systems will yield rich interactive functions through their redundant joints.

The following are the two central control issues for these systems: 1) robustly controlling interaction forces applied to contact points of interest and 2) compliantly adapting to arbitrary unknown external forces so that they do not disturb 1). For instance, the primary control objective for legged robots is to control the ground reaction force (GRF) due to its direct relationship to balancing. If 1) is the only control purpose, one can achieve force tracking by measuring the interaction forces to compute the joint angle deviation to reduce force tracking errors. This is position-based force control. With such an approach, however, achieving 2) becomes very difficult or nearly impossible.

Manuscript received January 21, 2008; revised May 14, 2008. First published November 11, 2008; current version published February 4, 2009. This paper was recommended for publication by Associate Editor K. Yamane and Editor H. Arai upon evaluation of the reviewers' comments. This work was supported by the National Institute of Information and Communications Technology (NICT), Japan.

This paper has supplementary downloadable material available at http://ieeexplore.ieee.org. This material includes video clips demostrating adaptation to unknown external forces, adaptation to uneven ground surface, adaptation to inclination of low friction, and impedance control test. The first video clip, i.e., adaptation to unknown external forces (Section II), shows that the robot can keep its balance under unknown external disturbances. This video also shows that the robot can interact with an external force applied to arbitrary contact points. The second video clip, i.e., adaptation to uneven ground surface (Section IV), shows that a humanoid robot is balancing on (unknown) uneven ground. The third video clip, i.e., adaptation to inclination of low friction (Section IV), shows that a humanoid robot is balancing on a wooden seesaw, and the fourth video clip, i.e., impedance control test (Section IV), shows the effectiveness of the impedance control between the feet. The size of the video is 12.5. MB. Contact sangho@atr.jp for further questions about this work.

The author is with the Advanced Telecommunications Research Institute International (ATR), Computational Neuroscience Laboratories, Kyoto 619-0288, Japan, and also with the Japan Science and Technology Agency (JST), International Cooperative Research Project (ICORP), Computational Brain Project, Saitama 332-0012, Japan (e-mail: sangho@atr.jp).

Color versions of one or more of the figures in this paper are available online at http://ieeexplore.ieee.org.

Digital Object Identifier 10.1109/TRO.2008.2006870